

This copy is for your personal, non-commercial use only.

If you wish to distribute this article to others, you can order high-quality copies for your colleagues, clients, or customers by [clicking here](#).

Permission to republish or repurpose articles or portions of articles can be obtained by following the guidelines [here](#).

The following resources related to this article are available online at www.sciencemag.org (this information is current as of February 17, 2011):

Updated information and services, including high-resolution figures, can be found in the online version of this article at:

<http://www.sciencemag.org/content/296/5567/535.full.html>

Supporting Online Material can be found at:

<http://www.sciencemag.org/content/suppl/2002/04/17/296.5567.535.DC1.html>

This article **cites 27 articles**, 15 of which can be accessed free:

<http://www.sciencemag.org/content/296/5567/535.full.html#ref-list-1>

This article has been **cited by** 301 article(s) on the ISI Web of Science

This article has been **cited by** 100 articles hosted by HighWire Press; see:

<http://www.sciencemag.org/content/296/5567/535.full.html#related-urls>

This article appears in the following **subject collections**:

Cell Biology

http://www.sciencemag.org/cgi/collection/cell_biol

Local Actin Polymerization and Dynamin Recruitment in SV40-Induced Internalization of Caveolae

Lucas Pelkmans, Daniel Püntener, Ari Helenius*

Simian virus 40 (SV40) utilizes endocytosis through caveolae for infectious entry into host cells. We found that after binding to caveolae, virus particles induced transient breakdown of actin stress fibers. Actin was then recruited to virus-loaded caveolae as actin patches that served as sites for actin "tail" formation. Dynamin II was also transiently recruited. These events depended on the presence of cholesterol and on the activation of tyrosine kinases that phosphorylated proteins in caveolae. They were necessary for formation of caveolae-derived endocytic vesicles and for infection of the cell. Thus, caveolar endocytosis is ligand-triggered and involves extensive rearrangement of the actin cytoskeleton.

The DNA virus SV40 has no envelope and differs from many other animal viruses in that it is endocytosed via caveolae instead of clathrin-coated vesicles during cell entry (1, 2). Caveolae are indentations in the plasma membrane thought to be involved in transcytosis, signal transduction, and the uptake of membrane components and extracellular ligands (3, 4). SV40 first binds to major histocompatibility complex class I antigens on the cell surface and is then trapped in caveolae that pinch off as vesicles that contain caveolin-1 and a single virus particle (2, 5). These vesicles fuse with larger, preexisting organelles, caveosomes, from which the viruses are sorted in larger, tubular vesicular carriers with the help of microtubules to the smooth endoplasmic reticulum (ER) (5, 6). The viruses exit the ER and enter the nucleus, most likely through nuclear pore complexes (7).

Here, we have examined whether SV40 actively induces caveolar endocytosis and, if so, what signals and cellular components are involved. Although it is known that caveolae have the capacity to pinch off as endocytic vesicles and that they can internalize a variety of ligands, the process does not seem to occur efficiently under normal culture conditions (8). Some type of perturbation is generally needed, such as cross-linking of caveolar membrane components, inhibition of phosphatases, or addition of hypertonic medium (9–12). SV40-loaded caveolae are internalized, whereas empty caveolae are not (5); this suggests that the virus can cause such a perturbation and thereby induce its own uptake.

Using a quantitative biochemical assay for internalization (13), we could observe that SV40 uptake started 20 min after binding (~1300 particles/cell) and continued for about 3 hours (Fig. 1A). Internalization leveled off after ~1500 particles/cell, although plenty of unbound virus particles were still

present in the medium. Apparently, there was only a single cycle of uptake.

As expected (1), the combination of the cholesterol-sequestering drug nystatin and the cholesterol synthesis inhibitor progesterone (Nys-Prog), which causes loss of rafts and caveolae (14), blocked virus uptake and infection by 90 to 95% (Fig. 1, A and C). Staurosporin (STP), a general kinase inhibitor, and genistein, a tyrosine kinase inhibitor that reduces SV40 infection (15) (Fig. 1C), reduced SV40 uptake by 70% (Fig. 1A). Okadaic acid (OA), a general phosphatase inhibitor, and vanadate, a tyrosine phosphatase inhibitor, enhanced initial binding of virus to the cells, increased uptake beyond a single cycle, and eliminated the initial lag (Fig. 1, A and B). Latrunculin A (LatA), an actin monomer-sequestering drug, and jasplakinolide (Jas), an actin polymer-stabilizing drug, reduced virus internalization by 60 to 65% (Fig. 1A). LatA reduced infection to a similar extent (Fig. 1C). Jas, however, blocked infection more efficiently than LatA, suggesting that, in addition to endocytosis, it interfered with later steps in the entry process (Fig. 1C). From these results, we concluded that, in addition to lipid rafts and caveolae, tyrosine kinases and actin must play a key role in internalization.

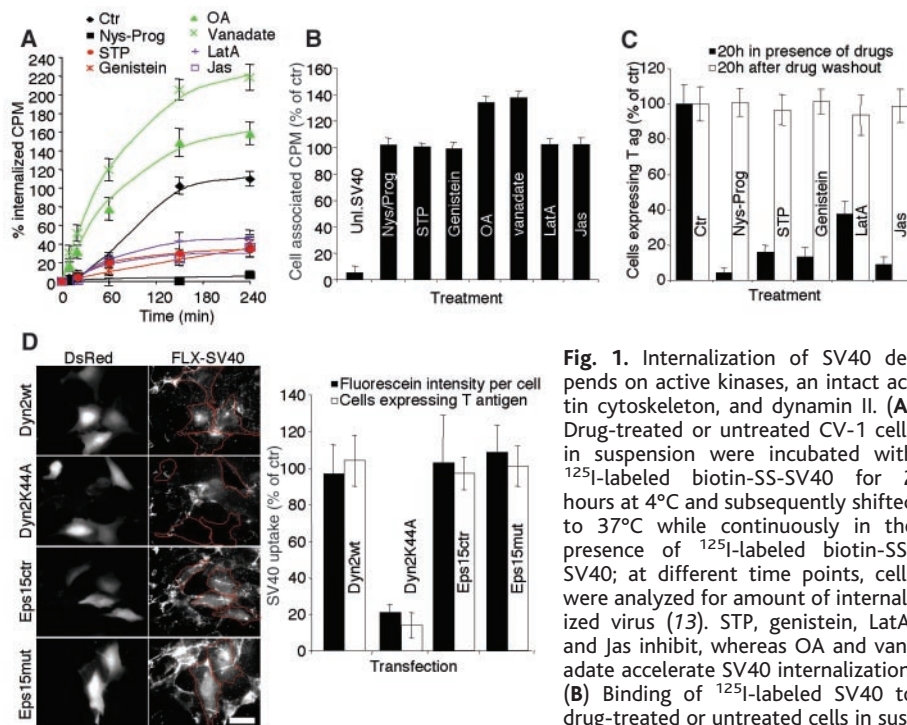


Fig. 1. Internalization of SV40 depends on active kinases, an intact actin cytoskeleton, and dynamin II. (A) Drug-treated or untreated CV-1 cells in suspension were incubated with ¹²⁵I-labeled biotin-SS-SV40 for 2 hours at 4°C and subsequently shifted to 37°C while continuously in the presence of ¹²⁵I-labeled biotin-SS-SV40; at different time points, cells were analyzed for amount of internalized virus (13). STP, genistein, LatA, and jas inhibit, whereas OA and vanadate accelerate SV40 internalization. (B) Binding of ¹²⁵I-labeled SV40 to drug-treated or untreated cells in suspension at 4°C. An excess of unlabeled SV40 (20 times) was used as a negative control (unl.SV40) (13). STP, genistein, LatA, and Jas do not influence binding, whereas OA and vanadate slightly increase binding. (C) Drug-treated cells were analyzed for expression of T antigen 20 hours after infection. As a control, the drugs were washed out, and cells were analyzed after an additional 20 hours. (D) SV40 uptake in cells cotransfected with DsRed-N1 and Dyn2wt, Dyn2K44A, Eps15DIIIΔ2 (Eps15ctr), or Eps15EΔ95/295 (Eps15mut) was quantified using the single-cell assay (13). Representative images are shown on the left. Infection was analyzed as in (C). Only Dyn2K44A inhibited SV40 internalization and infection. Scale bar, 50 μm.

Swiss Federal Institute of Technology Zurich (ETHZ), HPM1 Building, ETH Hönggerberg, CH-8093 Zurich, Switzerland.

*To whom correspondence should be addressed. E-mail: ari.helenius@bc.biol.ethz.ch

REPORTS

Using a quantitative “single-cell” assay for virus internalization (13), we tested the role of dynamin II, a member of the dynamin-GTPase family known to be involved in the internalization of clathrin-coated pits and caveolae (16, 17). The expression of a dominant-negative dynamin II construct with a mutation in the active GTPase site (dyn2K44A) (18) drastically reduced internalization and infectivity of the virus (Fig. 1D). A dominant-negative, truncated mutant of Eps15 (EΔ95/295), known to specifically block clathrin-coated pit assembly (19), did not block uptake or infection of SV40 (Fig. 1D). Thus, dynamin II is also involved in the infectious SV40 uptake by means of the caveolae.

Immediately after warming, tracking (13) of Alexa Fluor 594–labeled SV40 (AF-SV40) (20) revealed that individual viruses moved laterally in a random fashion (average speed, $0.17 \mu\text{m s}^{-1}$; average range, $4.04 \mu\text{m}$) [Fig. 2A; movie 1 (21)], until trapped within 10 min in immobile spots labeled with caveolin-1 tagged with green fluorescent protein (cav1-GFP) corresponding to caveolae (5) (average range, $0.67 \mu\text{m}$) (Fig. 2A; movies 2, 3, and 3A). LatA had a striking effect on this process; SV40 moved somewhat faster than in control cells (average speed, $0.24 \mu\text{m s}^{-1}$) and remained mobile even after reaching the spots positive for cav1-GFP (average range, $5.92 \mu\text{m}$) (Fig. 2A; supplementary Fig. 2,

movie 4). Evidently, the viruses were trapped in caveolae, but, instead of being stationary, these were now mobile (compare movies 5 and 5A). LatA had the same effect on cav1-GFP domains in the absence of SV40 (compare movies 6 and 6A). We concluded that actin filaments are not necessary for the diffusion of virus particles along the membrane or their sequestration into caveolae, but they do play a role in restricting the lateral mobility of caveolae.

In cells expressing GFP-β-actin, we observed that 10 to 20 min after virus entry was initiated, the number of actin stress fibers in the cell decreased dramatically (Fig. 2B). Instead, small actin patches and tails appeared

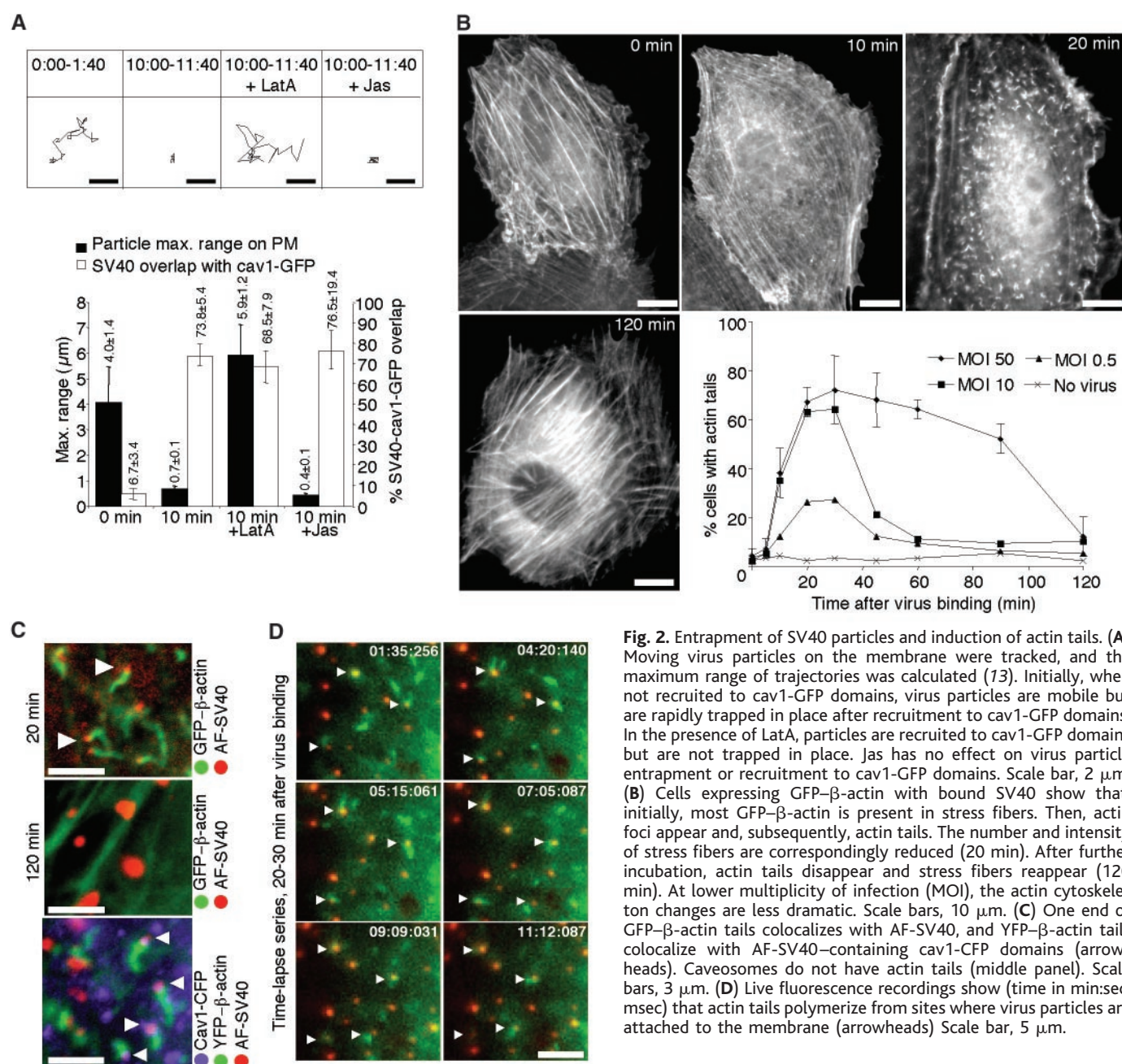


Fig. 2. Entrapment of SV40 particles and induction of actin tails. (A) Moving virus particles on the membrane were tracked, and the maximum range of trajectories was calculated (13). Initially, when not recruited to cav1-GFP domains, virus particles are mobile but are rapidly trapped in place after recruitment to cav1-GFP domains. In the presence of LatA, particles are recruited to cav1-GFP domains but are not trapped in place. Jas has no effect on virus particle entrapment or recruitment to cav1-GFP domains. Scale bar, $2 \mu\text{m}$. (B) Cells expressing GFP-β-actin with bound SV40 show that, initially, most GFP-β-actin is present in stress fibers. Then, actin foci appear and, subsequently, actin tails. The number and intensity of stress fibers are correspondingly reduced (20 min). After further incubation, actin tails disappear and stress fibers reappear (120 min). At lower multiplicity of infection (MOI), the actin cytoskeleton changes are less dramatic. Scale bars, $10 \mu\text{m}$. (C) One end of GFP-β-actin tails colocalizes with AF-SV40, and YFP-β-actin tails colocalize with AF-SV40-containing cav1-CFP domains (arrowheads). Caveosomes do not have actin tails (middle panel). Scale bars, $3 \mu\text{m}$. (D) Live fluorescence recordings show (time in min:sec:msec) that actin tails polymerize from sites where virus particles are attached to the membrane (arrowheads) Scale bar, $5 \mu\text{m}$.

REPORTS

on the upper surface of the cell, where most SV40 was located (Fig. 2B; movie 7). The changes were transient; after 120 min, GFP- β -actin displayed a normal pattern. The actin tails were on average 1.3 μ m long, and one end was generally tapered. The majority of tails ($65 \pm 11\%$) had a virus particle at their thick end (Fig. 2C, top panel). Live video recordings revealed that the tails used virus-associated actin patches as polymerization sites and that they were quite dynamic (Fig. 2D; movie 7, A and B).

In cells expressing yellow fluorescent protein (YFP) combined with β -actin (YFP- β -actin) and cyan fluorescent protein combined with cav1 (cav1-CFP), it became clear that the site for actin tail formation corresponded to cav1-CFP domains that had sequestered an AF-SV40 particle, namely, to virus-loaded caveolae (Fig. 2C, bottom panel). Whether the tails were present also on newly formed vesicular carriers could not be resolved. However, the caveosomes, into which the incoming viruses accumulated, were devoid of tails (Fig. 2C, middle panel).

The dissociation of stress fibers and the formation of actin tails were clearly SV40-induced; when fewer virus particles were

added, the changes were less prominent (Fig. 2B). In control cells without virus, no changes in the actin distribution were observed (movie 8).

To determine whether actin tail formation depended on viruses reaching the caveolae, we depleted cells of rafts and caveolae using Nys-Prog. No redistribution of actin was observed (Fig. 3), suggesting that SV40 must associate with caveolae or rafts to induce the changes in actin. Treatment with STP and genistein also inhibited the SV40-induced changes in actin. Treatment with STP and genistein also inhibited the SV40-induced changes in actin. Consistently, OA and vanadate accelerated the formation of actin tails when cells were exposed to SV40 (Fig. 3A). Note that OA (or vanadate) by itself induced the loss of actin stress fibers (Fig. 3A) but did not induce actin tails.

The actin and kinase inhibitors did not interfere with SV40 sequestration into caveolae (Fig. 3B and supplementary Fig. 2). This suggested that the virus normally activates the kinase(s) only when it has reached the caveolae. Binding AF-SV40 to cells expressing cav1-GFP, in fact, revealed that only

caveolae that contained viruses could be immunostained for phosphotyrosines (Fig. 4B). Cells expressing YFP- β -actin and cav1-CFP with bound SV40 showed, moreover, that caveolae that had actin tails were selectively immunostained (Fig. 4A, +SV40). In control cells without virus, phosphotyrosine staining was predominantly observed at focal adhesion contacts and not on cav1-CFP domains (Fig. 4A, -SV40). Thus, SV40 induces local tyrosine phosphorylation in caveolae, which correlates with actin tail formation.

When cells were pretreated with LatA, actin was recruited to plasma membrane-bound virus particles as a small patch, but no tail was formed (Fig. 5A). In control cells without virus, no such patches were observed. Apparently, actin patch formation induced by SV40 does not involve actin-actin interactions, whereas tail formation does. Live recordings showed that the virus-actin patches were mobile (movie 9). In contrast, pretreatment with Jas inhibited the dissociation of actin stress fibers, blocked the formation of actin patches, and prevented polymerization of actin tails (Fig. 5A).

The fate of the small fraction of viruses ($\sim 30\%$, Fig. 1A) that were endocytosed in the presence of Jas and LatA was distinct. In LatA-treated cells, these viruses were transported to caveosomes (Fig. 5B), and they were able to infect the cell, although with reduced efficiency (see Fig. 1C). This suggested that, although needed for efficient closure of the caveolae, an actin tail was not necessary for transport of the caveolar vesicles to caveosomes. In the presence of Jas, the virus-containing vesicles remained just below the cell surface (Fig. 5B), and the cells were not infected (see Fig. 1C). The presence of a Jas-stabilized, cortical actin cytoskeleton most likely prevented vesicle-transport further into the cytosol.

Finally, in cells expressing GFP-labeled dynamin II (Dyn2-GFP) (22), the Dyn2-GFP was visible at the surface only for brief periods of time (average 8 sec) as bright spots, resembling "blinking" lights in the video recording (movie 10). Dyn2K44A-GFP did not blink, but stayed as permanent bright spots on the membrane (23). When AF-SV40 particles were present, about 10% of the Dyn2-GFP spots were found to colocalize with them in a blinking manner (Fig. 5C; movie 11). When genistein was added to block the virus-induced signals, the blinking of Dyn2-GFP on virus particles was inhibited (Fig. 5C; movie 12). Blinking in other membrane domains was not affected (arrowheads). Without virus, some caveolin-1 domains contained Dyn2-GFP, but the fraction was less than 10% (23). Thus, like actin, dynamin II was recruited to virus-containing caveolae as a consequence of tyrosine kinase activation.

We have shown that SV40 induces its

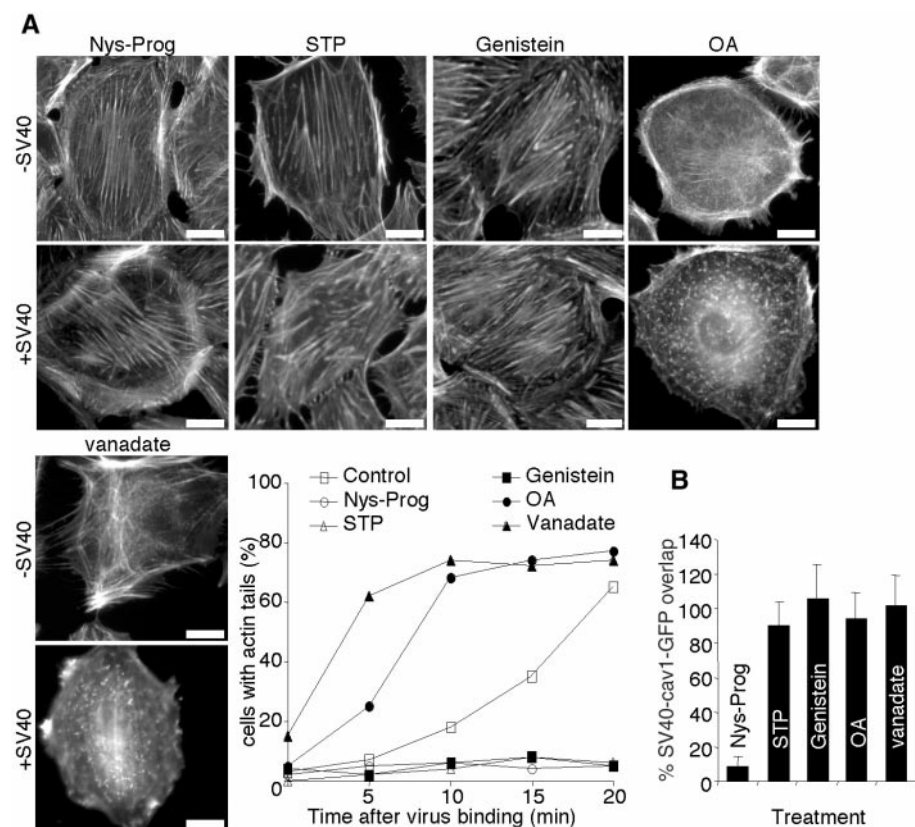


Fig. 3. SV40-induced actin tail formation depends on functional caveolae and active tyrosine kinases. (A) In cells expressing GFP- β -actin, Nys-Prog (by cholesterol depletion) and STP and genistein (by tyrosine kinase inhibition) block virus-induced actin changes. OA and vanadate (by tyrosine phosphatase inhibition) accelerate SV40-induced formation of actin tails. Scale bars, 5 μ m. (B) Nys-Prog treatment reduces overlap between AF-SV40 and cav1-GFP (determined as in Fig. 2A, bottom panel).

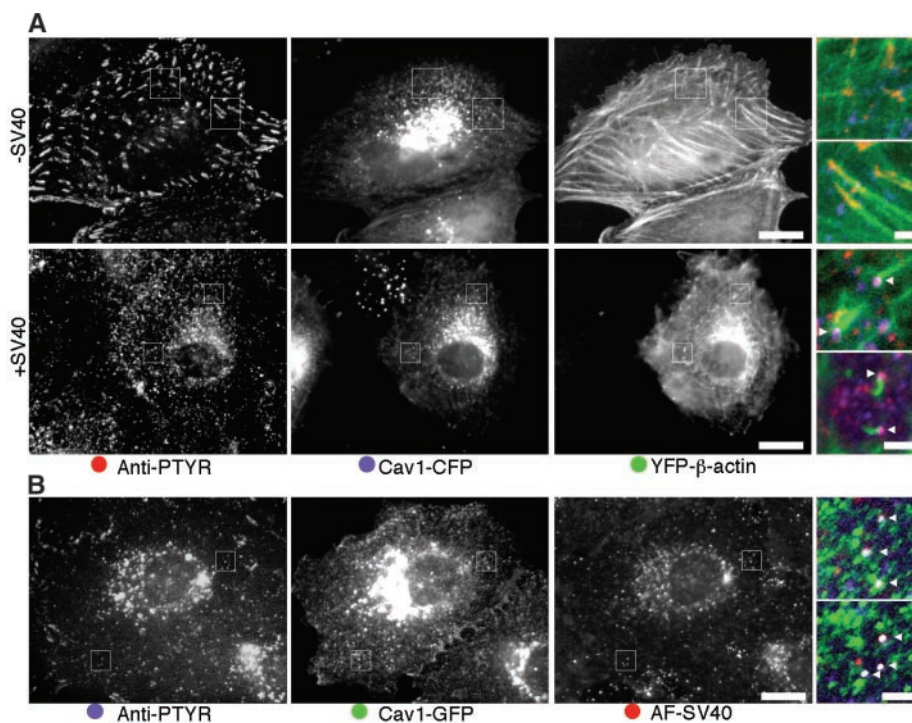


Fig. 4. SV40 particles induce tyrosine phosphorylation in virus-loaded caveolae. **(A)** Phosphotyrosine (PTYR) immunostaining in cells expressing YFP- β -actin and cav1-CFP is predominantly localized to focal adhesion sites, not to cav1-CFP domains. In cells having bound SV40, PTYR-staining on focal adhesion sites is lost and is now visible on cav1-CFP domains with actin tails (arrowheads). Scale bars, 5 μ m and 2 μ m (enlargements). **(B)** In cells expressing GFP- β -actin and having bound AF-SV40, PTYR-staining was visible on cav1-GFP domains that contained an SV40 particle. Overlap appears in white (arrowheads). Scale bars, 5 μ m and 2 μ m (enlargements).

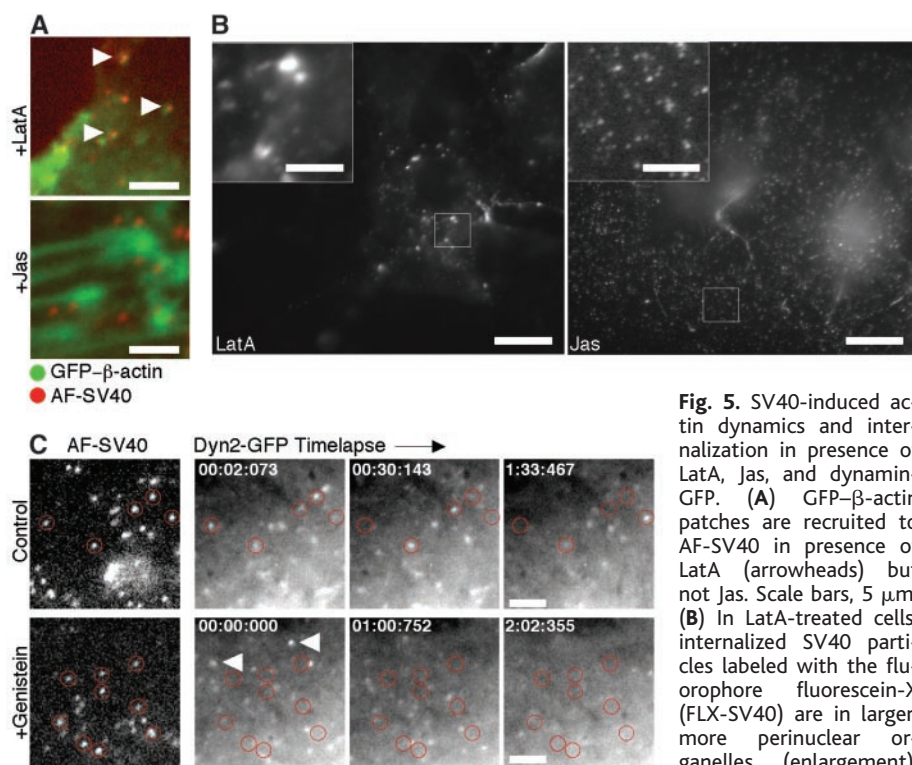


Fig. 5. SV40-induced actin dynamics and internalization in presence of LatA, Jas, and dynamin-GFP. **(A)** GFP- β -actin patches are recruited to AF-SV40 in presence of LatA (arrowheads) but not Jas. Scale bars, 5 μ m. **(B)** In LatA-treated cells, internalized SV40 particles labeled with the fluorophore fluorescein-X (FLX-SV40) are in larger, more perinuclear organelles (enlargement), whereas in Jas-treated cells, they are still visible as single particles, trapped in the periphery (enlargement). Scale bars, 20 μ m and 5 μ m (enlargements). **(C)** Live fluorescence recordings of cells expressing Dyn2-GFP show that Dyn2-GFP is recruited to membrane-bound AF-SV40 particles in a blinking manner (red circles). This is inhibited by genistein. Scale bars, 2.5 μ m.

own endocytic internalization. Once sequestered into caveolae, the virus particles trigger local tyrosine phosphorylation, leading to a complex series of transient changes in the caveolae and in the actin cytoskeleton. The first change is the disassembly of filamentous actin, followed by recruitment of actin and dynamin II to the cytosolic surface of the caveolae. Actin is first recruited as a patch that then serves as the site for actin tail formation. Actin and dynamin are important for the closure of the caveolae by membrane fission and for the free passage of vesicles deeper into the cytoplasm.

Actin plays an important role in phagocytosis (24) and it enhances the internalization of clathrin-coated pits (25). Actin tails, similar to those seen here, play a role in the inter- or intracellular mobility of several pathogens, such as *Listeria*, *Shigella*, and *Rickettsia* (26). The induction of actin tails by SV40 observed here resembles in many respects the well-characterized induction of actin tails by vaccinia virus (27). Both are mediated by virus particles bound to the outside surface of the plasma membrane (28), and both depend on tyrosine phosphorylation (29). Clearly, there are differences: SV40 uses actin tails for cell entry, whereas vaccinia virus induces them for cell exit and spread (30). In the case of SV40, the recruitment of actin must depend on cellular proteins located in caveolae; however, vaccinia virus uses a virus-encoded transmembrane protein (31).

Now what is needed is to identify the SV40-activated kinases and their substrates and to elucidate the signaling pathways that SV40 uses to activate caveolae, to recruit dynamin, and to reorganize actin. The mechanism may be related to that of dynamin recruitment to phosphatidylinositol-4-phosphate-kinase-induced actin tails on intracellular raft-enriched vesicles (32–34). More detailed analysis of this novel endocytic pathway and its regulation is necessary, because it is not only used by SV40 and other viruses (12, 35), but by bacteria (36), bacterial toxins, and several endogenous ligands and plasma membrane components.

References and Notes

1. H. Anderson, Y. Chen, L. Norkin, *Mol. Biol. Cell* **7**, 1825 (1996).
2. E. Stang, J. Kartenbeck, R. Parton, *Mol. Biol. Cell* **8**, 47 (1997).
3. G. Palade, *J. Appl. Physiol.* **24**, 1424 (1953).
4. R. Anderson, *Annu. Rev. Biochem.* **67**, 199 (1998).
5. L. Pelkmans, J. Kartenbeck, A. Helenius, *Nature Cell Biol.* **3**, 473 (2001).
6. J. Kartenbeck, H. Stukenbrok, A. Helenius, *J. Cell Biol.* **109**, 2721 (1989).
7. M. Yamada, H. Kasamatsu, *J. Virol.* **67**, 119 (1993).
8. P. Thomsen, K. Roepstorff, M. Stahlhut, B. van Deurs, *Mol. Biol. Cell* **13**, 238 (2002).
9. R. Parton, B. Joggerst, K. Simons, *J. Cell Biol.* **127**, 1199 (1994).
10. T. Aoki, R. Nomura, T. Fujimoto, *Exp. Cell Res.* **253**, 629 (1999).
11. Y. Kang, Y. Ko, J. Seo, *Exp. Cell Res.* **255**, 221 (2000).

12. Z. Richterova *et al.*, *J. Virol.* **75**, 10880 (2001).
13. Detailed methods as supplementary material are available on Science Online at www.sciencemag.org/cgi/content/full/296/5567/535/DC1.
14. K. Simons, D. Toomre, *Nature Rev Mol. Cell Biol.* **1**, 31 (2000).
15. Y. Chen, L. Norkin, *Exp. Cell Res.* **246**, 83 (1999).
16. J. Henley, E. Krueger, B. Oswald, M. McNiven, *J. Cell Biol.* **141**, 85 (1998).
17. P. Oh, D. McIntosh, J. Schnitzer, *J. Cell Biol.* **141**, 101(1998).
18. K. Fish, S. Schmid, H. Damke, *J. Cell Biol.* **150**, 145 (2000).
19. A. Benmerah, M. Bayrou, N. Cerf-Bensussan, A. Dautry-Varsat, *J. Cell Sci.* **112**, 1303 (1999).
20. Prepared as was TRX-SV40 (5), but using Alexa Fluor 594.
21. Movies and descriptions of them are found in supplementary material, available on Science Online at www.sciencemag.org/cgi/content/full/296/5567/535/DC1.
22. H. Cao, F. Garcia, M. McNiven, *Mol. Biol. Cell* **9**, 2595 (1998).
23. L. Pelkmans, A. Helenius, unpublished data.
24. R. May, L. Machesky, *J. Cell Sci.* **114**, 1061 (2001).
25. F. Brodsky, C. Chen, C. Kneuhl, M. Towler, D. Wakeham, *Annu. Rev. Cell Dev. Biol.* **17**, 517 (2001).
26. S. Dramsi, P. Cossart, *Annu. Rev. Cell Dev. Biol.* **14**, 137 (1998).
27. F. Frischknecht, M. Way, *Trends Cell Biol.* **11**, 30 (2001).
28. J. Rietdorf *et al.*, *Nature Cell Biol.* **3**, 992 (2001).
29. F. Frischknecht *et al.*, *Curr. Biol.* **9**, 89 (1999).
30. B. Ward, B. Moss, *J. Virol.* **75**, 11651 (2001).
31. F. Frischknecht *et al.*, *Nature* **401**, 926 (1999).
32. A. Rozelle *et al.*, *Curr. Biol.* **10**, 311 (2000).
33. E. Lee, P. De Camilli, *Proc. Natl. Acad. Sci. U.S.A.* **99**, 161 (2002).
34. J. Orth, E. Krueger, H. Cao, M. McNiven, *Proc. Natl. Acad. Sci. U.S.A.* **99**, 167 (2002).
35. V. Marjomaki *et al.*, *J. Virol.* **76**, 1856 (2002).
36. J. Shin, S. Abraham, *Microb. Infect.* **3**, 755 (2001).
37. The authors thank S. Schmid for suggesting the use of Tris(2-carboxyethyl)phosphine and for Dyn2 constructs, M. McNiven for dyn2-GFP constructs, and A. Benmerah and A. Dautry-Varsat for Eps15 constructs. This work was supported by the Swiss National Science Foundation and by ETHZ.

14 January 2002; accepted 11 March 2002

Role of Prostacyclin in the Cardiovascular Response to Thromboxane A₂

Yan Cheng,¹ Sandra C. Austin,¹ Bianca Rocca,¹ Beverly H. Koller,² Thomas M. Coffman,³ Tilo Grosser,¹ John A. Lawson,¹ Garret A. FitzGerald^{1*}

Thromboxane (Tx) A₂ is a vasoconstrictor and platelet agonist. Aspirin affords cardioprotection through inhibition of TxA₂ formation by platelet cyclooxygenase (COX-1). Prostacyclin (PGI₂) is a vasodilator that inhibits platelet function. Here we show that injury-induced vascular proliferation and platelet activation are enhanced in mice that are genetically deficient in the PGI₂ receptor (IP) but are depressed in mice genetically deficient in the TxA₂ receptor (TP) or treated with a TP antagonist. The augmented response to vascular injury was abolished in mice deficient in both receptors. Thus, PGI₂ modulates platelet-vascular interactions *in vivo* and specifically limits the response to TxA₂. This interplay may help explain the adverse cardiovascular effects associated with selective COX-2 inhibitors, which, unlike aspirin and nonsteroidal anti-inflammatory drugs (NSAIDs), inhibit PGI₂ but not TxA₂.

Prostacyclin (PGI₂) is the major product of cyclooxygenase (COX) catalyzed metabolism of arachidonic acid in macrovascular endothelium (1, 2). It is a potent inhibitor of platelet activation by all recognized agonists and a vasodilator. Biosynthesis of PGI₂ is increased in human syndromes of platelet activation (3), suggesting that it functions as a homeostatic response to accelerated platelet-vessel wall interactions. However, its importance *in vivo* has remained speculative. Recent studies of the coxibs, which are selective inhibitors of COX-2 (4) have suggested that this isozyme is a major source of PGI₂ under physiological conditions in humans (5, 6), perhaps reflective of COX-2 induction in endothelial cells by hemodynamic shear (7). PGI₂ synthase preferentially couples with

COX-2 rather than COX-1 in coexpression systems (8).

It is possible that PGI₂ modulates cardiovascular homeostasis in humans, as suggested by the outcome of a controlled comparison of a selective COX-2 inhibitor, rofecoxib, and an isoform nonselective inhibitor, naproxen (the VIGOR study). In this trial, rofecoxib was associated with a higher risk of myocardial infarction by a factor of 5 (9). Two mechanistic hypotheses have been advanced to explain these results: (i) A cardioprotective effect of naproxen, mediated by its inhibition of COX-1-dependent production of platelet TxA₂, and (ii) enhancement of the deleterious cardiovascular effects of TxA₂ in the patients on rofecoxib, which, in contrast to naproxen, inhibits only PGI₂ production, leaving TxA₂ unopposed (6).

To test the hypothesis that PGI₂ modulates the cardiovascular effects of TxA₂ *in vivo*, we generated mice with disordered expression of receptors for these eicosanoids and monitored the response to vascular injury. Both PGI₂ and TxA₂ activate G protein-coupled receptors, the prostacyclin receptor (the IP) and the thromboxane receptor (the TP), respectively (10, 11).

Others have shown that IP knockout mice (IPKOs) do not develop spontaneous thrombosis but are more susceptible to thrombotic stimuli than their wild-type (WT) littermates (12). TPKOs, by contrast, exhibit a mild bleeding tendency (13). Both IPKOs and TPKOs are normotensive.

Initially, we studied the impact of IP deletion on the proliferative response to catheter-induced carotid vascular injury. This model involves passage of a polyamide catheter containing a fine wire down the common carotid artery, causing endothelial denudation, neointimal formation, and vascular smooth muscle cell proliferation (14, 15). Neointimal proliferation was not observed 2 weeks after surgery in sham-treated mice, but it was induced by injury in both IPKOs and their WT littermates (15). Deletion of the IP resulted in an enhanced proliferative response to injury: the intima-to-media ratio increased significantly in the IPKOs (Fig. 1A). The percentage of luminal stenosis was also increased after injury in the IPKOs [Web table 1 (15)]. We also assessed intimal cellular proliferation by bromodeoxyuridine (BrdU) labeling. There was no significant labeling in the intima or media of uninjured WTs. Injury caused a marked increase in labeling of both intimal and medial cells in WTs. However, intimal and medial proliferation was enhanced in IPKOs (Fig. 1B). In humans, vascular angioplasty is associated with an increase in platelet activation, reflected by urinary excretion of the Tx metabolite (Tx-M), 2,3-dinor-TxB₂ (16). Patients undergoing coronary angioplasty are given aspirin, which suppresses TxA₂ formation and reduces the periprocedural rate of myocardial infarction by ~50% (17). We found that catheter-induced carotid injury in the mouse also results in a significant increase in Tx biosynthesis (Fig. 1C), which was augmented in the IPKOs compared with IPWTs (Fig. 1D). These data support the hypothesis that PGI₂ modulates platelet activation by TxA₂ *in vivo*.

To address the functional importance of TxA₂ in this mouse model, we investigated the effect of S18886, a highly selective, long acting TP antagonist activity (18). We measured the impact of TP antagonism on the response to

¹Center for Experimental Therapeutics, 153 Johnson Pavilion, 3620 Hamilton Walk, University of Pennsylvania School of Medicine, Philadelphia, PA 19104-6084, USA. ²Department of Medicine, University of North Carolina, Chapel Hill, NC 27559, USA. ³Department of Medicine, Duke University, Durham, NC 27705, USA.

*To whom correspondence should be addressed. E-mail: garret@spirit.gcr.upenn.edu